Inorganic Chemistry

Article

pubs.acs.org/IC

Quantum Chemical Determination of Novel C_{82} Monometallofullerenes Involving a Heterogeneous Group

Hong Zheng,[†] Xiang Zhao,*[,†] Ling He,[†] Wei-Wei Wang,[‡] and Shigeru Nagase[‡]

[†]Institute for Chemical Physics & Department of Chemistry, Xi'an Jiaotong University, Xi'an 710049, China

[‡]Fukui Institute for Fundamental Chemistry, Kyoto University, Kyoto 606-8103, Japan

Supporting Information

ABSTRACT: By means of density functional theory methods together with statistical thermodynamic analysis, the C_{82} monometallofullerenes including special heterogeneous triangular clusters were theoretically probed for the first time. Despite having analogous structures, the YCN@C_{82} and TbCN@C_{82} series exhibit dissimilar thermodynamic stabilities, which lead to different components of experimental products. Significant relationship between the thermodynamic stabilities and geometry structures of C_{82} metallofullerenes is disclosed. Studies of the electronic configurations of MCN@C_{82} species not only explain their redox potentials but also recover complicated interaction mechanisms within them. In addition, predictions of the optical spectra of observed MCN@C_{82} species coincide with experimental detections well, indicating that simulations for other structures will be helpful for future characterization of these cyanoclusterfullerenes.

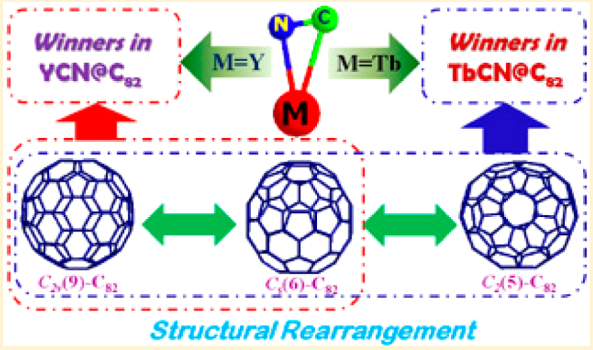

INTRODUCTION

Ever since the discovery of the first endohedral metallofullerene (EMF) La@C_{82} in 1991,[1] numerous EMF molecules encapsulating various metal atoms or metalloclusters have been synthesized. Presenting novel physical and chemical properties brought by the entrapped atoms or clusters, the EMFs have much wider potential applications than pure carbon cages in electronics, photovoltaics, and biomedicine.[2−8] As a common kind of EMF that has been extensively studied, the monometallofullerenes (mono-EMFs) had been believed to occur only in the form of M@C_{2n} ($2n$ = 80, 88, 96)[25] for a long time until the synthesis of a new kind of mono-EMF YCN@$C_s(6)$-C_{82} in 2013.[9] The YCN@$C_s(6)$-C_{82} structure, which could also be recognized as a cyano-clusterfullerene molecule with fewer metal atoms than in previous cases (such as $Sc_3CN@C_{80}$ and $Sc_3CN@C_{78}$),[10,11] has a special triangular YCN cluster determined by the single-crystal X-ray diffraction crystallography.

As for the EMFs containing lanthanide atoms, although most lanthanide atoms have been successfully encapsulated, further research on the lanthanide-based EMFs is still rather scarce due to the difficult isolation and characterization of them in experiment. Hence, a quantum chemical method would be the best way to investigate the chemical/physical properties of the lanthanide-based EMF systems. So far, previous theoretical studies have uncovered the significant properties of some lanthanide-based EMFs such as $La_2@C_{72}$/La@C_{82},[12,13] $Ce_2@C_{72}$/Ce@C_{82},[14,15] $Gd_3N@C_{2n}$/Gd_2C_{2n},[16−18] Yb@C_{2n},[19−21] $Dy_2@C_{100}$,[22] Lu_2C_{2n},[23,24] $M_3N@C_{2n}$,etc. Nevertheless, many more lanthanide-based EMFs still lack detailed studies because of huge computational work and difficult theoretical treatment of the lanthanide atoms having 4f electrons.

Apart from YCN@$C_s(6)$-C_{82}, another cyanoclusterfullerene TbCN@C_{82} has been synthesized by Yang's group recently,[26] whose geometry structure was determined by X-ray crystallographic study, which disclosed a different carrier cage of $C_2(5)$-C_{82}. Note that among the reported C_{82} metallofullerenes, the $C_2(5)$-C_{82} and $C_s(6)$-C_{82} cages, as well as another two cages $C_{2v}(9)$-C_{82} and $C_{3v}(8)$-C_{82}, have been frequently discovered in experiments, and the products were always found to be mixtures of certain kinds of isomers involving these cages.[27−31] It seems that the compositions of C_{82} metallofullerenes may have dependence on the endohedral clusters, and unfortunately, experimental observation usually has a shortage of comprehensive insight of the EMF structures. For many EMFs, limited by various factors, not all the isomers can be isolated and characterized. Take MCN@C_{82} (M = Y, Tb), for example; there are some questions that cannot be answered by the present experimental results: why do the two molecules having analogous metalloclusters involve different C_{82} cages? Are YCN@$C_s(6)$-C_{82} and TbCN@$C_2(5)$-C_{82} the sole synthesized products of the two types of EMF systems? If not, what are the structures of other isomers? Moreover, the MCN@C_{82} model, whose encapsulated cluster containing three types of elements is the first pattern of heterogeneous endohedral metallocluster, is still lacking deep insight of geometric and electronic natures.

Received: August 7, 2014
Published: December 3, 2014

   dx.doi.org/10.1021/ic501911z | Inorg. Chem. 2014, 53, 12911−12917

Therefore, the profound perception on the thermodynamic stabilities of these cyanoclusterfullerenes, which directly relates to the composition of experimental product, can only be provided by theoretical methods. The determination of the EMF structures from theoretical aspect normally has dependence on the relative potential energies of the EMF isomers, which, however, cannot always supply satisfying results due to a non-negligible enthalpy−entropy effect within the formation temperature interval of fullerene.[32]

The interaction between the metalloclusters and fullerene cages is another significant aspect in the discussion of EMF systems. Many researchers are used to depicting the electronic configuration of an EMF molecule as $(MC)^{m+}@C_{2n}{}^{m-}$ (MC represents metallocluster), which suggests an ionic bonding mechanism between the metallocluster and fullerene cage in the form of electron transfer.[33] However, some studies have pointed out that, to some extent, a covalent bonding mechanism can also exist in the EMF molecules. On one hand, the metal atoms readily become cations due to donation of certain valence electrons, and therefore ionic bonding occurs in the EMF molecules. On the other hand, covalent bonding mechanism, which is also called "electron backdonation", originating from orbital overlap between the metal valence orbitals and cage orbitals,[34] reveals complex interaction within the EMF systems.

In this paper, complete features of thermodynamic stabilities of $MCN@C_{82}$ (M = Y, Tb) series were depicted by means of combined methodologies of quantum chemistry and statistical mechanics. To disclose the interaction mechanisms within the $MCN@C_{82}$ isomers (especially the $TbCN@C_{82}$ structures), investigations of the MCN−cage interaction as well as the inner bonding of TbCN cluster were performed. To obtain deep insight into the optical properties of $MCN@C_{82}$ EMFs, the UV−visible−near-IR (UV−vis−NIR) and ^{13}C NMR spectra of the most important $MCN@C_{82}$ isomers were simulated and compared with the experimental detections.

EXPERIMENTAL SECTION

Since there is only one metal atom in the $MCN@C_{82}$ (M = Y, Tb) species, and the MCN clusters were presumed to contribute two electrons to the C_{82} cages, giving rise to a C_{82}^{2-} valence state, the energetics for all those 744 C_{82}^{2-} anions ($C_{3v} \times 2$, $C_{2v} \times 5$, $C_2 \times 58$, $C_s \times 23$, $C_1 \times 656$), including nine anions obeying the isolated pentagon rule (IPR)[35,36] and 735 non-IPR anions with 1−2 pentagon adjacency (PA) fragments, were first screened at the AM1[37] level. Then, 12 cages with relative energies less than 30 kcal/mol as well as one previously reported non-IPR cage $C_s(39663)$-C_{82} were chosen as the candidate cages and reoptimized by the hybrid density functional theory (DFT) B3LYP[38−40] with 6-31G* basis set (Supporting Information, Table S1). For comparison, another two lowest-energy C_{82}^{2-} anions with two PAs are also included in Supporting Information, Table S1. Optimizations on the $YCN@C_{82}$ structures were first performed at B3LYP/BSI level (BSI = 6-31G*∼Lanl2DZ, where 6-31G* basis set for C and N atoms and Lanl2DZ basis set with the corresponding pseudopotential for Y atom). For comparison, another hybrid functional theory PBE1PBE[41] was also employed for the reoptimizations of partial $YCN@C_{82}$ structures possessing relative energies less than 30 kcal/mol with the same basis set. The ground-state structures of the $TbCN@C_{82}$ series were investigated at B3LYP/BSII level (BSII = 6-31G*∼MWB54, where 6-31G* basis set for C and N atoms and effective core potential basis set MWB54 for Tb atom). Specially, several important $MCN@C_{82}$ isomers were reoptimized by BP86[38,42] method combining with triple-ζ plus polarization (TZP) basis set for the C, N, and Y atoms (MWB54 was still used for Tb atom). Rotational−vibrational partition functions for relative concentration investigation of the $YCN@C_{82}$ and $TbCN@C_{82}$ series were provided by structural and vibrational analyses calculated at B3LYP/BSI and B3LYP/BSII levels of theory, respectively. The time-dependent (TD) DFT calculations on the most important $TbCN@C_{82}$ isomers were carried out utilizing Perdew−Burke−Ernzerhof (PBE) functional theory and BSII basis set. The ^{13}C NMR spectrum simulations for both kinds of $MCN@C_{82}$ species employing the gauge including atomic orbital method (GIAO) method were also produced by PBE method with a larger basis set for carbon atoms (6-311G* for C atoms, 6-31G* for N atom, and Lanl2DZ/MWB54 for Y/Tb atoms as before). All computational works above were performed by the Gaussian03 program package excepting the calculations at BP86/TZP and BP86/TZP∼MWB54 levels, which were carried out by the Gaussian09 package (see Supporting Information).

RESULTS AND DISCUSSION

Relative Stabilities and Structural Peculiarities of $MCN@C_{82}$ (M = Y, Tb) Series. The energy sequence of C_{82}^{2-} anions, showing good accordance between the results of semiempirical and DFT methods, supports $C_{2v}(9)$-C_{82}^{2-} anion as the lowest-energy cage (Supporting Information, Table S1). $C_s(6)$-C_{82} and $C_2(5)$-C_{82} cages become the second and third lowest-energy anions with small relative energies of 2.1 and 4.0 kcal/mol, respectively. Note that the most stable non-IPR C_{82}^{2-} anion is predicted to be $C_s(39701)$-C_{82}^{2-}, which was omitted by a previous report.[43] The $C_{3v}(7)$-C_{82} cage presents a pretty large highest occupied molecular orbital−lowest unoccupied molecular orbital (HOMO−LUMO) gap (1.73 eV) in anion state, implying an evidence energy difference between the LUMO and LUMO+1 orbitals in neutral $C_{3v}(7)$-C_{82} cage.

In the case of $YCN@C_{82}$ EMFs, the energy sequence of the $YCN@C_{82}$ series is predicted to be similar to that of C_{82}^{2-} anions, implying little influence of encapsulating YCN cluster to the energetic differences. As shown in Table 1, the $C_{2v}(9)$-C_{82} cage exhibits the lowest potential energies in both series after accepting the MCN clusters. In the $YCN@C_{82}$ series, $YCN@C_s(6)$-C_{82} and $YCN@C_2(5)$-C_{82} species have small relative energies within 5 kcal/mol, while other species lie more than 11 kcal/mol above the $YCN@C_{2v}(9)$-C_{82} structure according to the first two levels of theory. Reoptimizations at BP86/TZP level have further confirmed the sequence of the first four isomers (Table 1a). The most energetically stable non-IPR $YCN@C_{82}$ isomer is $YCN@C_s(39701)$-C_{82}, which is 22.9 kcal/mol higher than $YCN@C_{2v}(9)$-C_{82}. The sequence of HOMO−LUMO gaps of $YCN@C_{82}$ series also presents good accordance with that of the C_{82}^{2-} anions, indicating that two-electron transfer from YCN cluster to carbon cage occurs in the $YCN@C_{82}$ isomers.

Analogous energy and HOMO−LUMO sequences were found between the $YCN@C_{82}$ and $TbCN@C_{82}$ series, meaning the variation of metal atom might have slight influence on both thermodynamic and kinetic stabilities of the two types of $MCN@C_{82}$ series (Table 1b). However, the potential energies at 0 K cannot reflect the real relative stabilities of those isomers forming at high temperatures, and in many cases reported previously,[32,44,45] certain higher-energy fullerene isomers may surpass the lowest-energy isomer in relative contribution within the formation temperature interval. Here, to determine the composition of the experimental products, statistical thermodynamic analyses considering enthalpy−entropy effect were performed for both $MCN@C_{82}$ series.

As depicted in Figure 1a, the $YCN@C_{2v}(9)$-C_{82} structure, sharing the largest relative concentrations at all temperatures, is followed by the $YCN@C_s(6)$-C_{82} structure, and both of them

dx.doi.org/10.1021/ic501911z | Inorg. Chem. 2014, 53, 12911−12917

Table 1. Relative Energies (in kcal/mol) and HOMO−LUMO Gaps (in eV) of MCN@C_{82} (M = Y, Tb) Isomers at Various Levels of Theory

(a) calculation results of YCN@C_{82} series

		B3LYP/BSI		PBE1PBE/BSI		BP86/TZP	
sym. no.[a]	PA	ΔE	gap	ΔE	gap	ΔE	gap
$C_{2v}(9)$	0	0.0	1.54	0.0	1.74	0.0	0.69
$C_s(6)$	0	3.0	1.56	2.8	1.76	2.8	0.70
$C_2(5)$	0	4.8	1.78	4.3	1.99	3.9	0.96
$C_{3v}(7)$	0	11.7	2.00	11.5	2.22	11.8	1.11
$C_{3v}(8)$	0	11.3	1.08	11.7	1.27		
$C_2(3)$	0	18.0	1.38	17.5	1.57		
$C_2(1)$	0	22.3	1.37	21.2	1.57		
$C_s(39\,701)$	1	22.9	1.34	21.7	1.55		
$C_1(39\,686)$	1	28.8	1.19	28.1	1.40		
$C_s(4)$	0	29.5	0.84	30.7	0.92		
$C_s(2)$	0	31.3	1.25				
$C_s(39\,704)$	1	37.4	1.26				
$C_s(39\,663)$	1	42.7	0.81				

(b) calculation results of TbCN@C_{82} series

		B3LYP/BSI		BP86/TZP∼MWB54	
sym. no.[a]	PA	ΔE	gap	ΔE	gap
$C_{2v}(9)$	0	0.0	1.54	0.0	0.70
$C_s(6)$	0	3.3	1.56	2.8	0.70
$C_2(5)$	0	5.0	1.78	4.3	0.96
$C_{3v}(7)$	0	11.8	2.00		
$C_{3v}(8)$	0	12.0	1.09		
$C_2(3)$	0	18.9	1.36		
$C_2(1)$	0	22.8	1.37		
$C_s(39\,701)$	1	23.9	1.35		
$C_1(39\,686)$	1	30.0	1.20		
$C_s(4)$	0	32.0	0.72		
$C_s(2)$	0	32.1	1.23		
$C_s(39\,704)$	1	39.0	1.28		
$C_s(39\,663)$	1	44.2	0.83		

[a]Fowler number is used for the IPR isomers, while spiral number is used for the non-IPR isomers.

have no interchange with other isomers. Evidently, the YCN@C_{82} curves are analogous to Boltzmann distribution excepting for interchanges among two isomers of no thermodynamic importance. Thus, it is reasonable to conclude that the YCN@$C_{2v}(9)$-C_{82} structure should also be an experimental product besides the reported YCN@$C_s(6)$-C_{82} structure. Moreover, because of small contribution within all temperature intervals, the YCN@$C_2(5)$-C_{82} isomer might occur as a trace in experiment.

The situation of TbCN@C_{82} series is complicated with significant stability interchanges among lower-energy isomers (Figure 1b). The curve of the TbCN@$C_{2v}(9)$-C_{82} structure slides down abruptly after 500 K and is surpassed by that of the TbCN@$C_s(6)$-C_{82} structure at ∼2000 K, then it intersects with the curve of TbCN@$C_2(5)$-C_{82} at ∼4800 K. The TbCN@$C_s(6)$-C_{82} structure keeps the largest concentration at all higher temperature intervals, implying that it would be a main product within the fullerene formation temperatures (2000−3000 K).[32] In addition, the concentrations of TbCN@$C_{2v}(9)$-C_{82} and TbCN@$C_s(6)$-C_{82} structures are ∼40%, while that of TbCN@$C_2(5)$-C_{82} reaches 20% at 2000 K, giving rise to a ratio of these three isomers as 2:2:1 and suggesting a mixture of these structures in experiment.

Generally, the component of YCN@C_{82} is mainly composed of YCN@$C_{2v}(9)$-C_{82} and YCN@$C_s(6)$-C_{82} species, while TbCN@$C_{2v}(9)$-C_{82} and TbCN@$C_s(6)$-C_{82} as well as TbCN@$C_2(5)$-C_{82} play important roles in the product of TbCN@C_{82}. That all previously reported isomers have outstanding stabilities and large concentrations reflects good accordance with the experimental observations. The optimized geometry structures of YCN@$C_s(6)$-C_{82} and TbCN@$C_2(5)$-C_{82} are in accord with the experimental detections, excepting for longer C≡N bonds (both are 1.183 Å), which are more comparable to the cases of $Sc_3CN@C_{80}$ and $Sc_3CN@C_{78}$[10,11] than the unusual experimental observations (0.935 Å in YCN@$C_s(6)$-C_{82} and 0.94(5) Å in TbCN@$C_2(5)$-C_{82}).[9,26] The optimization of the HCN molecule carried out at B3LYP/6-31G* level, which predicted a rather accurate C≡N bond length (1.160 Å) compared with the real value (115.8 pm), suggests high accuracy of our calculations and that the single X-ray diffraction determinations on C≡N bond are, to some extent, discussable. After all, for the CN group, up to now no evidence has confirmed a higher bond order and a shorter bond length than triple bond.

The MCN^{2+} cluster tends to keep a linear M−N≡C form rather than M−C≡N form in free condition according to our theoretical calculations. Triangular pattern is unachievable because the Y/Tb atom is hard to bond with the C and N atoms at the same time due to strong electrostatic repulsion

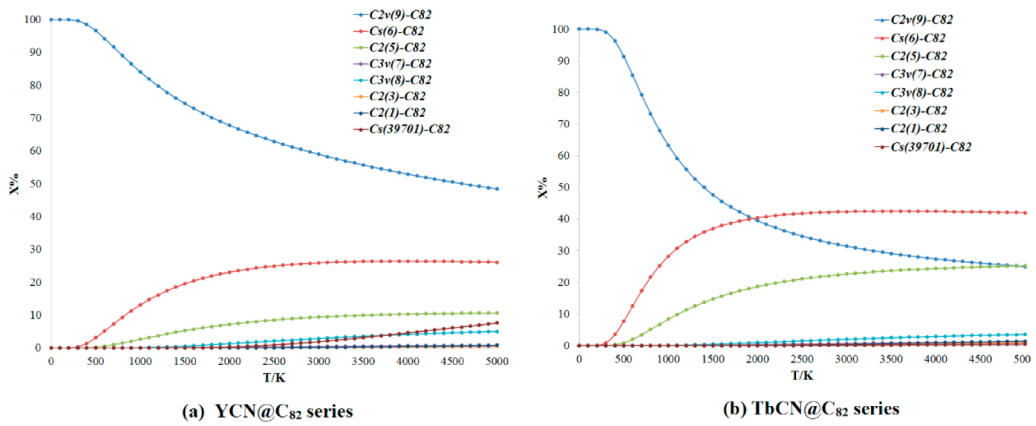

(a) YCN@C_{82} series (b) TbCN@C_{82} series

Figure 1. Relative concentrations of low-energy MCN@C_{82} (M = Y, Tb) isomers.

dx.doi.org/10.1021/ic501911z | Inorg. Chem. 2014, 53, 12911−12917

between the metal and carbon atoms, which both possess positive charges. However, when entrapped in the C_{82} cages, the MCN clusters are bent to various extents (Figure 2) with

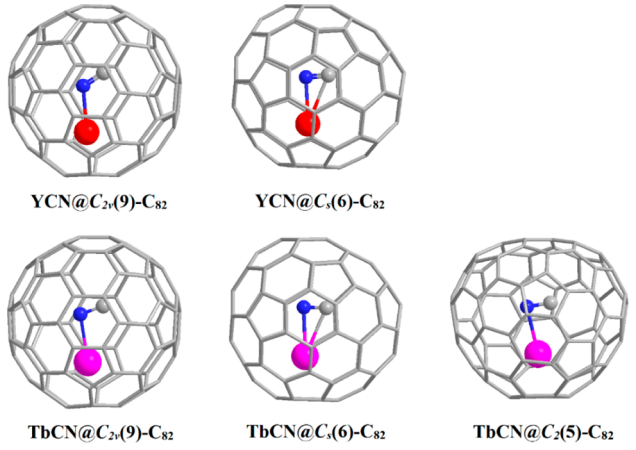

Figure 2. Geometry structures of main MCN@C_{82} (M = Y, Tb) isomers. The N atom is colored blue, while Y and Tb atoms are of red and purple colors, respectively.

∠MNC angles ranging from 86.06° to 117.97°. For each C_{82} cage, the corresponding YCN@C_{82} species resembles the TbCN@C_{82} species in topological geometry, and the metal atoms tend to be located near a hexagon ring of the C_{82} cage that lies on the plane or axis of symmetry. Both the triangular MCN clusters in MCN@C_s(6)-C_{82} molecules deviate from the plane of symmetry with similar small dihedral angles. However, a C_s point group in YCN@C_s(6)-C_{82} has been confirmed by ^{13}C NMR,[9] implying that the CN moiety can freely swing in the C_s(6)-C_{82} cage. Hence, its isostructure TbCN@C_s(6)-C_{82} can also possess a C_s symmetry. Analogously, for C_2(5)-C_{82} and C_{2v}(9)-C_{82} cages, their point groups of static geometry structures are, apparently, destroyed by the metalloclusters. In view of the case of C_s(6)-C_{82} EMF systems, it is superficial to say that they have no symmetry in the form of EMF due to the possibility of an internal dynamic mechanism of MCN clusters. Supporting Information, Figure S1 reveals that the TbCN cluster can easily rotate along the C_2 axes of C_2(5)-C_{82} and C_{2v}(9)-C_{82} cages with rather small energy barriers (1.1 kcal/mol in both TbCN@C_2(5)-C_{82} and TbCN@C_{2v}(9)-C_{82}), and it is reasonable to assume that the YCN@C_{2v}(9)-C_{82} species being isostructural with TbCN@C_{2v}(9)-C_{82} can also possess such internal dynamic mechanism. Therefore, all the main MCN@C_{82} species should maintain the point groups of their pristine cages.

On the basis of numerous experimental observations and theoretical predictions, structural relationships among pristine cages of certain EMFs, in the form of cage growth/shrink[46−49] and Stone−Wales (SW) rearrangement,[50] have been discovered. Balch et al. claimed that four experimentally discovered C_{82} cages would be possible intermediate structures during the fullerene formation process toward a top-down mechanism.[49] In fact the C_2(5)-C_{82} cage omitted in their work also has structural connection with C_s(6)-C_{82} cage through a one-step SW rearrangement (Figure 3). Another non-IPR cage C_s(39 663)-C_{82} mentioned in ref 49 is not independent of other famous C_{82} cages but can give C_s(6)-C_{82} cage by means of an SW rearrangement. Hence, all discovered C_{82} cages have been connected, implying significant relation between the thermodynamic stabilities and topological geometries of C_{82} EMFs. Being different from other medium- or large-size fullerene series whose discovered isomers are not always closely related by simple SW rearrangement, the C_{82} fullerene is fairly special for the close structural relationships among all C_{82} EMFs.

Electronic Properties of MCN@C_{82} (M = Y, Tb) Structures. According to Yang's report, it appears that different EMF structures with the same carrier cage and valence state (such as TbCN@C_2(5)-C_{82} and Yb@C_2(5)-C_{82}) present similar electrochemical properties.[26] Moreover, the electronic structures of YCN@C_{82} and TbCN@C_{82} species having the same carrier cage are rather similar because of their analogous frontier orbital distributions and energy levels (Supporting Information, Figure S2); namely, these two types of cyanoclusterfullerenes should exhibit similar electronic properties. Here, we focus on the main TbCN@C_{82} structures and analyze the frontier orbital interaction between the TbCN cluster and C_{82} cages. Shown in Supporting Information, Figure S3, the LUMO orbitals of the three neutral hollow C_{82} cages become the HOMO orbitals of their EMF structures after

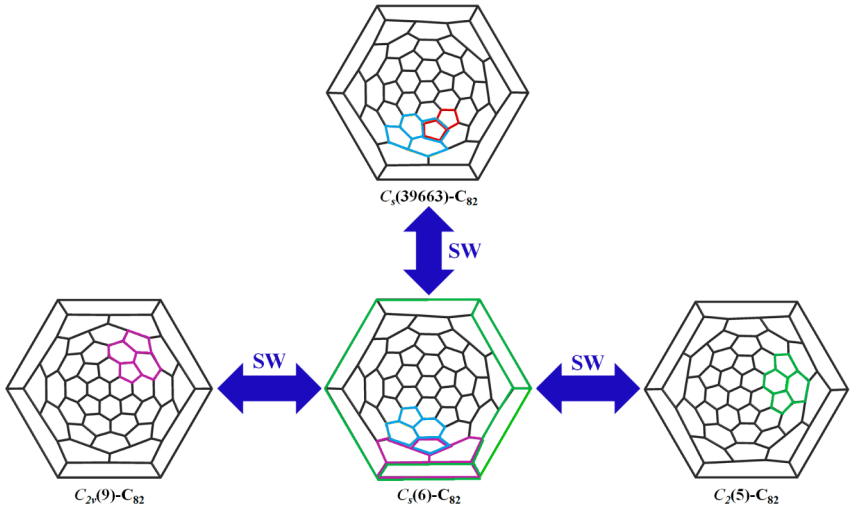

Figure 3. Schlegel diagrams of certain structurally related C_{82} cages. The PA fragment of C_s(39 663)-C_{82} cage is colored with red, and the fragments referred to each SW rearrangement are of the same color.

dx.doi.org/10.1021/ic501911z | Inorg. Chem. 2014, 53, 12911−12917

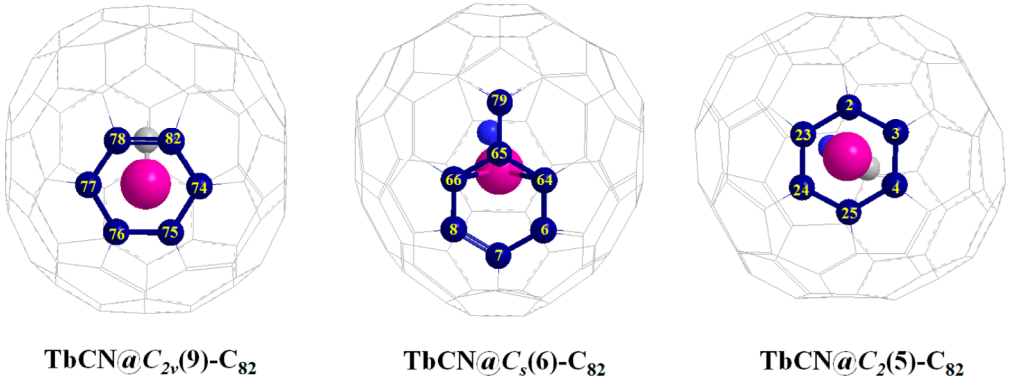

Figure 4. Serial numbers of carbon atoms (colored with blue) in C_{82} cages that have large Tb−N Mayer bond order values.

accepting two electrons from the TbCN cluster, giving rise to a $(TbCN)^{2+}@C_{82}^{2-}$ valence state. The same electron-transfer mechanism can be expected in the YCN@C_{82} species because of the analogous frontier orbitals of this series compared to those of the TbCN@C_{82} species. Such ionic bond is the basis of the interaction between the MCN clusters and C_{82} cages. However, there would also be covalent bonding features within these cyanoclusterfullerenes according to previous studies on EMFs. Further analysis of covalent bonding within the main TbCN@C_{82} isomers will be introduced later.

The redox potentials of C_{82} EMFs can be reasonably explained from the viewpoint of frontier orbital analysis. The orbital energy levels, whose absolute values strongly depend on the employed theory method, can conform to the reality with their relative values. The HOMO−LUMO gap of TbCN@C_2(5)-C_{82} is 0.22 eV larger than that of two MCN@C_s(6)-C_{82} species, exhibiting good accordance with the difference between the $\Delta E_{gap,EC}$ values of C_2(5)-C_{82} and C_s(6)-C_{82} EMFs in ref 26. In addition, the separation difference (0.5 V) between the first and third reduction steps of C_2(5)-C_{82} and C_s(6)-C_{82} EMFs can be explained by the fact that the energy gap between LUMO and LUMO+1 orbitals (LUMO−LUMO+1 gap) in TbCN@C_2(5)-C_{82} is 0.43 eV narrower than that in MCN@C_s(6)-C_{82} (Supporting Information, Figures S2 and S3). The small separation between the first two reduction steps and the last two reduction steps could be attributed to electron paring energy brought by the second electron filling in the LUMO or LUMO+1 orbital. As for the MCN@C_{2v}(9)-C_{82} structures, now that their HOMO−LUMO gaps are close to those of MCN@C_s(6)-C_{82} species and their LUMO−LUMO+1 gaps are notably larger than those of other MCN@C_{82} species, their $\Delta E_{gap,EC}$ values would be ∼1.15 V, and large separations between the first and third reduction steps could be expected.

To obtain deeper interpretations of the bonding behavior within the TbCN@C_{82} isomers, natural bond orbital (NBO) analysis was performed at B3LYP/6-31G*∼MWB28 level. Because of the computational complexity of the ECP basis with a smaller effective core, only the TbCN@C_{2v}(9)-C_{82} structure was analyzed successfully, in which the Tb atom possesses an electron configuration of $6s^{0.18}4f^{8.10}5d^{0.87}6p^{0.44}$. In view of a $4f^9 6s^2$ configuration in neutral Tb atom, the significant decrease in 6s and 4f orbitals reveals that three electrons detach from the Tb atom, two of which transfer to carbon cage, and the third one may correspond to the increased electronic populations in CN moiety (increased by 0.37 e) and the unoccupied 5d and 6p orbitals. Besides, the electron backdonation from carbon cage is another factor leading to the large electronic populations in the 5d and 6p orbitals of Tb atom. According to our previous work, for a typical EMF series, the electronic populations of metal atoms in various isomers were always predicted to be of little difference,[48,51] and hence other TbCN@C_{82} isomers should possess similar electronic populations.

Furthermore, the covalent bonding features of TbCN@C_{82} series involving Mayer bond orders and bonding critical point (BCP) indicators, the latter of which is based on quantum theory of atoms in molecules (QTAIM) and has been used for a variety of EMF systems,[52,53] were obtained by means of the MULTIWFN 3.2.1 program.[54] Here, we still focus on the bonding behavior of Tb atom toward the CN moiety and the carbon atoms nearby.

It is revealed that the Tb−N Mayer bond order values, ranging from 0.581 to 0.593, possess positive correlation with the Tb−N distances (Supporting Information, Table S2). Although the distances between Tb and the carbon atom (C84) of CN moiety are close to or even longer than other Tb−C distances, the Tb−C84 Mayer bond orders (0.480−0.559) are much larger than other bond orders referring to the cage carbon atoms. Considering that the total orders of Tb bonding to CN moiety in the three cages are as large as 1.073−1.140, significant Tb-CN interaction can be concluded in the form of covalent bonding. The interaction between Tb and cage atoms shows delocalization features like those of previous reports:[55,56] having bond orders ranging from 0.166 to 0.270, those carbon atoms near the Tb atom (Figure 4) compose small regions and possess total bond orders from 1.356 to 1.547, suggesting remarkable orbital overlaps between the Tb atom and C_{82} cages.

The BCPs referred to Tb−cage and Tb−CN bonds are shown in Supporting Information, Figure S4, and the corresponding parameters are collected in Supporting Information, Table S2. Small and positive electron density and Laplacian values predicted in all BCPs show similarities to other EMF systems.[52,57,58] For the Tb−N BCPs, despite of two positive energy densities in TbCN@C_s(6)-C_{82} and TbCN@C_2(5)-C_{82}, probably ascribed to longer Tb−N distances (compared to TbCN@C_{2v}(9)-C_{82}) that may cause weaker interaction, small ellipticities of the three Tb−N BCPs indicate noteworthy covalent interaction in the Tb−N bonds. It is revealed that all carbon atoms involved in the Tb−C BCPs belong to the blue regions in Figure 4, and it seems that there are inconspicuous differences between the Tb−N and Tb−C BCPs in terms of electronic densities and ratio of the absolute value of the potential energy density to the kinetic energy density ($|V|/G$). However, larger ellipticities of the Tb−C

dx.doi.org/10.1021/ic501911z | Inorg. Chem. 2014, 53, 12911−12917

BCPs disclose characteristic increasing π character of these Tb−C bonds. In addition, owing to the internal dynamic mechanisms in the TbCN@C_{82} structures as mentioned above, some other carbon atoms, also included in the blue regions, are actually equivalent to the carbon atoms having Tb−C BCPs, and hence they may present the same covalent features with Tb atom. This phenomenon further affirms the delocalization features of the metal-cage covalent interaction.

Optical Spectra of Main MCN@C_{82} Species. To aid future characterizations of the MCN@C_{82} EMFs, simulations of the UV−vis−NIR and ^{13}C NMR spectra of the main MCN@C_{82} isomers were carried out. Evidently, the simulated UV−vis−NIR spectrum of the TbCN@C_s(6)-C_{82} structure (Figure 5) is almost the same as that of the YCN@C_s(6)-C_{82} structure.[9]

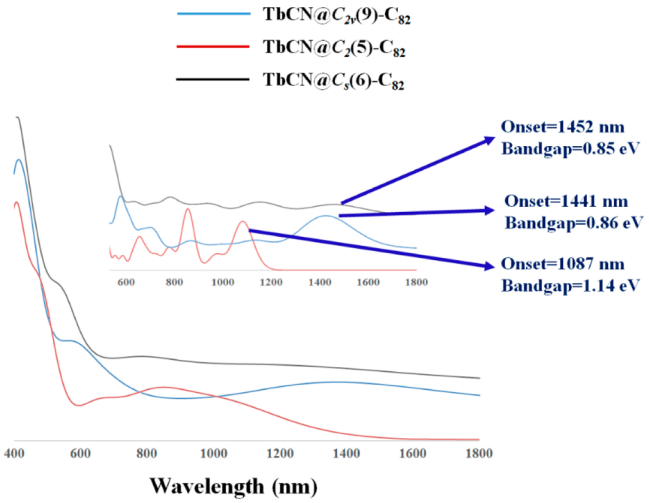

Figure 5. Simulated UV−vis−-NIR spectra of main TbCN@C_{82} isomers.

The peaks of the TbCN@C_2(5)-C_{82} structure in the UV and visible regions accord with experimental observations, and the first excitation predicted at 1.14 eV is quite comparable with the reported optical band gap (1.0 eV).[26] The computed first excitation of the TbCN@C_{2v}(9)-C_{82} structure locates at 0.86 eV since its HOMO−LUMO gap is nearly that of the TbCN@C_s(6)-C_{82} structure. The excitations of the YCN@C_{2v}(9)-C_{82} structure should highly resemble those of TbCN@C_{2v}(9)-C_{82} because of their analogous electronic structures.

The calculations of ^{13}C NMR spectra of MCN@C_s(6)-C_{82} and MCN@C_{2v}(9)-C_{82} species were performed for comparison and are shown in Supporting Information, Figure S5. All the chemical shifts fall into the aromatic region, and the shift sections of MCN@C_{2v}(9)-C_{82} species (130−155 ppm) are narrower than those of MCN@C_s(6)-C_{82} species (125−155 ppm). Obviously, there is little difference between the two kinds of metallofullerenes with the same cages. Although, presumably ascribed to certain factors (such as solvent effect), the long lines lying in the higher field of the YCN@C_s(6)-C_{82} structure are predicted to be somewhat different from experimental observations,[9] the whole shift section (125.5−152.9 ppm) and the shifts of short lines (125.5−143.6 ppm) can coincide with the experimental data well.

CONCLUSIONS

Extensive studies of the MCN@C_{82} (M = Y, Tb) series by means of DFT calculations in conjunction with statistical thermodynamic analysis disclose overall perspectives of the MCN@C_{82} products, in which several new stable isomers besides the reported ones have been discovered, and notable differences of the thermodynamic stabilities of these two sorts of cyanoclusterfullerenes have been revealed: the YCN@C_{2v}(9)-C_{82} and YCN@C_s(6)-C_{82} species are predicted to be the most stable isomers and the main products in electric arc, while three TbCN@C_{82} isomers, namely, TbCN@C_{2v}(9)-C_{82} and TbCN@C_s(6)-C_{82} as well as TbCN@C_2(5)-C_{82}, would be dominant in the synthesized TbCN@C_{82} EMFs due to their outstanding stabilities. Special geometrical connections via simple SW rearrangement among all the C_{82} cages discovered heretofore have been uncovered, reflecting a significant relationship between the geometrical structures and thermodynamic stabilities of the C_{82} EMFs. The frontier orbital analysis not only defines the electron transfer in the main MCN@C_{82} structures, but also provides excellent explanations for the redox potentials detected in experiment. Especially, a detailed investigation on the covalent bonding behavior within TbCN@C_{82} structures recovers significant Tb−CN and Tb−cage covalent features, which is another factor bringing in the change of electronic configuration of the Tb atom excepting electron transfer. Finally, the predictions of the optical spectra of the main MCN@C_{82} isomers provide important information for the future characterizations of the MCN@C_{82} EMFs. In conclusion, this work would be not only of importance for the interpretation of thermodynamic stabilities and electronic/geometric peculiarities of the novel cyanoclusterfullerenes but also valuable for further experimental and theoretical research on the EMFs encapsulating heterogeneous groups.

ASSOCIATED CONTENT

Supporting Information

Author lists of Gaussian03 and Gaussian09 program packages, relative energies and HOMO−LUMO gaps of partial C_{82}^{2-} isomers, interatomic distances, Mayer bond orders and BCP parameters for Tb−N and Tb−cage interactions, shapes and energy levels (eV) of frontier orbital of main MCN@C_{82} isomers, frontier orbital diagram of the main TbCN@C_{82} isomers, rotation modes of TbCN cluster in the main TbCN@C_{82} structures, BCPs (indicated with red rings) between the Tb atom and nonmetallic atoms nearby in the main TbCN@C_{82} structures, simulated ^{13}C NMR spectra of MCN@C_{82} isomers, and coordinates of the main MCN_2@C_{82} isomers. This material is available free of charge via the Internet at http://pubs.acs.org.

AUTHOR INFORMATION

Corresponding Author

*Fax: +86 29 8266 8559. Phone: +86 29 8266 5671. E-mail: xzhao@mail.xjtu.edu.cn.

Notes

The authors declare no competing financial interest.

ACKNOWLEDGMENTS

This work was supported by the National Natural Science Foundation of China (No. 21171138), National Key Basic Research Program of China (No. 2012CB720904), and China Postdoctoral Science Foundation (No. 2013M532038).

REFERENCES

(1) Chai, Y.; Cuo, T.; Jin, C.; Haufler, R. E.; Chibante, L. P. F.; Fure, J.; Wang, L.; Alford, J. M.; Smalley, R. E. *J. Phys. Chem.* **1991**, *95*, 7564−7568.
(2) Wilson, L. J.; Cagle, D. W.; Thrash, T. P.; Kennel, S. J.; Mirzadeh, S.; Alford, J. M.; Ehrhardt, G. J. *Coord. Chem. Rev.* **1999**, *190*−*192*, 199−207.
(3) Akasaka, T.; Nagase, S. *Endofullerenes: A New Family of Carbon Clusters;* Kluwer Academic Publishers: Dordrecht, The Netherlands, 2002.
(4) Dunsch, L.; Yang, S. *Small* **2007**, *3*, 1298−1320.
(5) Akasaka, T.; Wudl, F.; Nagase, S. *Chemistry of Nanocarbons;* Wiley-Blackwell: London, 2010.
(6) Lu, X.; Akasaka, T.; Nagase, S. *Chem. Commun.* **2011**, *47*, 5942−5957.
(7) Lu, X.; Akasaka, T.; Nagase, S. *Acc. Chem. Res.* **2013**, *46*, 1627−1635.
(8) Popov, A. A.; Yang, S.; Dunsch, L. *Chem. Rev.* **2013**, *113*, 5989−6113.
(9) Yang, S.; Chen, C.; Liu, F.; Xie, Y.; Li, F.; Jiao, M.; Suzuki, M.; Wei, T.; Wang, S.; Chen, Z.; Lu, X.; Akasaka, T. *Sci. Rep.* **2013**, *3*, 1487.
(10) Wang, T. S.; Feng, L.; Wu, J. Y.; Xu, W.; Xiang, J. F.; Tan, K.; Ma, Y. H.; Zheng, J. P.; Jiang, L.; Lu, X.; Shu, Chun. Y.; Wang, C. R. *J. Am. Chem. Soc.* **2010**, *132*, 16362−16364.
(11) Wu, J.; Wang, T.; Ma, Y.; Jiang, L.; Shu, C.; Wang, C. *J. Phys. Chem. C* **2011**, *115*, 23755−23759.
(12) Slanina, Z.; Chen, Z.; Schleyer, P. v. R.; Uhlík, F.; Lu, X.; Nagase, S. *J. Phys. Chem. A* **2006**, *110*, 2231−2234.
(13) Feng, M.; Shi, Y.; Lin, C.; Zhao, J.; Liu, F.; Yang, S.; Petek, H. *Phys. Rev. B* **2013**, *88*, 075417.
(14) Yamada, M.; Wakahara, T.; Tsuchiya, T.; Maeda, Y.; Akasaka, T.; Mizorogi, N.; Nagase, S. *J. Phys. Chem. A* **2008**, *112*, 7627−7631.
(15) Muthukumar, K.; Larsson, J. A. *J. Phys. Chem. A* **2008**, *112*, 1071−1075.
(16) Alegret, N.; Chaur, M. N.; Santos, E.; Rodríguez-Fortea, A.; Echegoyen, L.; Poblet, J. M. *J. Org. Chem.* **2010**, *75*, 8299−8302.
(17) Yang, T.; Zhao, X.; Li, L. S.; Zheng, J. J.; Gao, W. Y. *ChemPhysChem.* **2012**, *13*, 449−452.
(18) Guo, Y. J.; Yang, T.; Nagase, S.; Zhao, X. *Inorg. Chem.* **2014**, *53*, 2012−2021.
(19) Slanina, Z.; Uhlík, F.; Nagase, S. *J. Phys. Chem. A* **2006**, *110*, 12860−12863.
(20) Yang, T.; Zhao, X.; Xu, Q.; Zhou, C. H.; He, L.; Nagase, S. *J. Mater. Chem.* **2011**, *21*, 12206−12209.
(21) Yang, T.; Zhao, X.; Nagase, S. *J. Phys. Chem. C* **2012**, *116*, 21640−21645.
(22) Yang, T.; Zhao, X.; Nagase, S. *Phys. Chem. Chem. Phys.* **2011**, *13*, 5034−5037.
(23) Yang, T.; Zhao, X.; Osawa, E. *Chem.—Eur. J.* **2011**, *17* (37), 10230−10234.
(24) Zheng, H.; Zhao, X.; Wang, W. W.; Dang, J. S.; Nagase, S. *J. Phys. Chem. C* **2013**, *117*, 25195−25204.
(25) Aparicio-Angles, X.; Alegret, N.; Clotet, A.; Rodríguez-Fortea, A.; Poblet, J. M. *J. Phys. Chem. C* **2013**, *117*, 12916−12921.
(26) Liu, F.; Wang, S.; Guan, J.; Wei, T.; Zeng, M.; Yang, S. *Inorg. Chem.* **2014**, *53*, 5201−5205.
(27) $(Y_2C_2)@C_{82}$ system: (a) Inoue, T.; Tomiyama, T.; Sugai, T.; Okazaki, T.; Suematsu, T.; Fujii, N.; Utsumi, H.; Nojima, K.; Shinohara, H. *J. Phys. Chem. B* **2004**, *108*, 7573−7579. (b) Inoue, T.; Tomiyama, T.; Sugai, T.; Shinohara, H. *Chem. Phys. Lett.* **2003**, *382*, 226−231.
(28) $(Sc_2C_2)@C_{82}$ system: (a) Nishibori, E.; Ishihara, M.; Takata, M.; Sakata, M.; Ito, Y.; Inoue, T.; Shinohara, H. *Chem. Phys. Lett.* **2006**, *433*, 120−124. (b) Iiduka, Y.; Wakahara, T.; Nakajima, K.; Nakahodo, T.; Tsuchiya, T.; Maeda, Y.; Akasaka, T.; Yoza, K.; Liu, M. T. H.; Mizorogi, N.; Nagase, S. *Angew. Chem., Int. Ed.* **2007**, *46*, 5562−5564. (c) Yamazaki, Y.; Nakajima, K.; Wakahara, T.; Tsuchiya, T.; Ishitsuka, M. O.; Maeda, Y.; Akasaka, T.; Waelchli, M.; Mizorogi, N.; Nagase, S. *Angew. Chem., Int. Ed.* **2008**, *47*, 7905−7908.
(29) $Sc_2@C_{82}$ system: (a) Wang, C. R.; Inakuma, M.; Shinohara, H. *Chem. Phys. Lett. 300* **1999**, *300*, 379−384. (b) Mercado, B. Q.; Stuart, M. A.; Mackey, M. A.; Pickens, J. E.; Confait, B. S.; Stevenson, S.; Easterling, M. L.; Valencia, R. n.; Rodríguez-Fortea, A.; Poblet, J. M.; Balch, A. L.; Olmstead, M. M. *J. Am. Chem. Soc.* **2010**, *132*, 12098−12105.
(30) $Yb@C_{82}$ system: Suzuki, M.; Slanina, Z.; Mizorogi, N.; Lu, X.; Nagase, S.; Olmstead, M. M.; Balch, A. L.; Akasaka, T. *J. Am. Chem. Soc.* **2012**, *134*, 18772−18778.
(31) Chen, N.; Chaur, M. N.; Moore, C.; Pinzón, J. R.; Valencia, R.; Rodríguez-Fortea, A.; Poblet, J. M.; Echegoyen, L. *Chem. Commun.* **2010**, *46*, 4818−4820.
(32) Slanina, Z. *Int. Rev. Phys. Chem.* **1987**, *6*, 251−267.
(33) Campanera, J. M.; Bo, C.; Olmstead, M. M.; Balch, A. L.; Poblet, J. M. *J. Phys. Chem. A* **2002**, *106*, 12356−12364.
(34) Liu, D.; Hagelberg, F.; Park, S. S. *Chem. Phys.* **2006**, *330*, 380−386.
(35) Fowler, P. W.; Manolopoulos, D. E. *An Atlas of Fullerenes;* Clarendon Press: Oxford, U.K., 1995.
(36) Kroto, H. W. *Nature* **1987**, *329*, 529−531.
(37) Dewar, M. J. S.; Zoebisch, E.; Healy, E. F.; Stewart, J. J. P. *J. Am. Chem. Soc.* **1985**, *107*, 3902−3909.
(38) Becke, A. D. *Phys. Rev. A* **1988**, *38*, 3098−3100.
(39) Becke, A. D. *J. Chem. Phys.* **1993**, *98*, 5648−5652.
(40) Lee, C.; Yang, W.; Parr, R. G. *Phys. Rev. B* **1988**, *37*, 785−789.
(41) Perdew, J. P.; Burke, K.; Ernzerhof, M. *Phys. Rev. Lett.* **1996**, *77*, 3865.
(42) Perdew, J. P. *Phys. Rev. B* **1986**, *33*, 8822−8824.
(43) Liu, X.; Li, L.; Liu, B.; Wang, D.; Zhao, Y.; Gao, X. *J. Phys. Chem. A* **2012**, *116*, 11651−11655.
(44) Slanina, Z.; Lee, S. L.; Uhlik, F.; Adamowicz, L.; Nagase, S. *Theor. Chem. Acc.* **2007**, *117*, 315−322.
(45) Zhao, X.; Gao, W. Y.; Yang, T.; Zheng, J. J.; Li, L. S.; He, L.; Cao, R. J.; Nagase, S. *Inorg. Chem.* **2012**, *51*, 2039−2045.
(46) Popov, A. A.; Dunsch, L. *J. Am. Chem. Soc.* **2007**, *129*, 11835−11849.
(47) Yang, T.; Zhao, X.; Nagase, S. *J. Phys. Chem. C* **2012**, *116*, 21640−21645.
(48) Zheng, H.; Zhao, X.; Ren, T.; Wang, W. W. *Nanoscale* **2012**, *4*, 4530−4536.
(49) Zhang, J.; Bowles, F. L.; Bearden, D. W.; Ray, W. K.; Fuhrer, T.; Ye, Y.; Dixon, C.; Harich, K.; Helm, R. F.; Olmstead, M. M.; Balch, A. L.; Dorn, H. C. *Nat. Chem.* **2013**, *5*, 880−885.
(50) Stone, A. J.; Wales, D. J. *Chem. Phys. Lett.* **1986**, *128*, 501−503.
(51) Zheng, H.; Zhao, X.; Wang, W. W.; Yang, T.; Nagase, S. *J. Chem. Phys.* **2012**, *137*, 014308.
(52) Popov, A. A.; Dunsch, L. *Chem.—Eur. J.* **2009**, *15*, 9707−9729.
(53) Guo, Y. J.; Gao, B. C.; Yang, T.; Nagase, S.; Zhao, X. *Phys. Chem. Chem. Phys.* **2014**, *16*, 15994−16002.
(54) Lu, T.; Chen, F. W. *J. Comput. Chem.* **2012**, *33*, 580−592.
(55) Cortés-Guzmán, F.; Bader, R. F. W. *Coord. Chem. Rev.* **2005**, *249*, 633−662.
(56) Bader, R. F. W.; Matta, C. F. *Inorg. Chem.* **2001**, *40*, 5603−5611.
(57) Kobayashi, K.; Nagase, S. *Chem. Phys. Lett.* **1999**, *302*, 312−316.
(58) Kobayashi, K.; Nagase, S. *Chem. Phys. Lett.* **2002**, *362*, 373−379.